Single crystal growth and magnetism of Sr_3NaIrO_6 and Sr_3AgIrO_6: Tracking the $J = 0$ ground state of Ir^{5+}

Peng-Bo Song (宋鹏博),[1,2] Zhiwei Hu,[3] Su-Yang Hsu,[4] Jin-Ming Chen,[4] Jyh-Fu Lee,[4] Shan-Shan Miao (苗杉杉),[1] You-Guo Shi (石友国),[1,2,5,*] and Hai L. Feng (冯海)[1,5,†]

[1]*Beijing National Laboratory for Condensed Matter Physics and Institute of Physics, Chinese Academy of Sciences, Beijing 100190, China*
[2]*Center of Materials Science and Optoelectronics Engineering, University of Chinese Academy of Sciences, Beijing 100190, China*
[3]*Max Planck Institute for Chemical Physics of Solids, Dresden 01187, Germany*
[4]*National Synchrotron Radiation Research Center, Hsinchu 30076, Taiwan, Republic of China*
[5]*Songshan Lake Materials Laboratory, Dongguan, Guangdong 523808, China*

(Received 26 July 2022; accepted 22 September 2022; published 29 September 2022)

Single crystals of Sr_3NaIrO_6 and Sr_3AgIrO_6 have been successfully grown using hydroxides flux. Sr_3NaIrO_6 and Sr_3AgIrO_6 crystallize in the K_4CdCl_6-type structure with the space group R-3c (no. 167). Sr_3NaIrO_6 and Sr_3AgIrO_6 are electrically insulating with estimated activation gaps of 0.68 and 0.80 eV, respectively. Sr_3NaIrO_6 and Sr_3AgIrO_6 show paramagnetic behavior down to 2 K. In this work, the observed effective moments, $\mu_{\rm eff}$, for Sr_3NaIrO_6 single crystals are $0.31\mu_{\rm B}$ for $H\perp c$ and $0.28\mu_{\rm B}$ for $H||c$, which are much smaller than that of $0.49\mu_{\rm B}$ previously reported for the polycrystalline Sr_3NaIrO_6 samples. For Sr_3AgIrO_6 single crystals, a much larger value of $\mu_{\rm eff} = 0.57\mu_{\rm B}$ is observed as compared with Sr_3NaIrO_6 single crystals. The x-ray absorption spectroscopy and low-temperature specific heat data indicate that the Ir in Sr_3NaIrO_6 has an almost pure Ir^{5+} valence state, while the Ir in Sr_3AgIrO_6 is slightly lower than +5. The estimated low limits of magnetic impurity Ir^{4+} are about ~1.7% and ~9.2% for Sr_3NaIrO_6 and Sr_3AgIrO_6, respectively. These magnetic impurities are likely to fully explain the observed $\mu_{\rm eff}$ values for Sr_3NaIrO_6 and Sr_3AgIrO_6 single crystals, supporting the $J = 0$ ground state of Ir^{5+} in Sr_3NaIrO_6 and Sr_3AgIrO_6.

DOI: 10.1103/PhysRevMaterials.6.094415

I. INTRODUCTION

In 3d transition metal oxides, the valence electrons are strongly correlated and the Hubbard U plays an important role [1–5]. In comparison with 3d electrons, the orbitals of 5d electrons are more extended and the U in the 5d system becomes weaker while the spin-orbit coupling (SOC) becomes much stronger due to their larger atomic number [6,7]. In the strong SOC regime, the SOC can split three t_{2g} orbitals in the octahedral crystal field into an upper $j = 1/2$ doublet and a lower $j = 3/2$ quadruplet [8,9]. For example, in tetravalent iridate Sr_2IrO_4 (Ir^{4+}: $5d^5$) the SOC-assisted Mott-insulating state is explained with the $J = 1/2$ ground state [9]. Resonant inelastic x-ray scattering measurements on pentavalent osmates (Os^{5+} : $5d^3$) reveal the SOC controlled $J = 3/2$ ground state [10]. In such a scenario, if there are four 5d electrons filling the lower quadruplet, the ground state should be $j = 0$. Long-range magnetic orders reported in Ir^{5+} ($5d^4$) double perovskite oxides Sr_2YIrO_6 and Ba_2YIrO_6 with effective moment ($\mu_{\rm eff}$) of 0.91 $\mu_{\rm B}$/Ir and 1.44 $\mu_{\rm B}$/Ir, respectively, raise concerns about the ground state of $5d^4$ oxides [11,12]. These results have been challenged by other studies reporting that no magnetic order was found in Ba_2YIrO_6 [13] and Sr_2YIrO_6 [14] down to ~430 mK. Studies on A_2YIrO_6 (A = Sr, Ba) and other Ir^{5+} double perovskite oxides generally reveal a weak paramagnetic behavior with small $\mu_{\rm eff}$ values of 0.19–0.63 $\mu_{\rm B}$/Ir [13–25] which are much lower than the theoretical spin-only $\mu_{\rm eff} = 2.83\,\mu_{\rm B}$/Ir demonstrating a SOC dominated ground state. The origin of these finite magnetic moments is still ambiguous. Quench of the $J = 0$ state for Ir^{5+} due to IrO_6 octahedra distortion in Sr_2YIrO_6 was proposed by Cao *et al.* [11]. However, this scenario cannot explain the paramagnetic moment observed in cubic Ba_2YIrO_6 where there is no structural distortion, and the studies on $Ba_{2-x}Sr_xYIrO_6$ do not find correlations between $\mu_{\rm eff}$ values and the degree of structural distortions [19,26]. The existence of magnetic impurities has been suggested by studies on Sr_2YIrO_6 [14] and Ba_2YIrO_6 [17]. Fuchs *et al.* confirmed the existence of Ir^{4+} and Ir^{6+} magnetic defects which are responsible for the magnetism in Ba_2YIrO_6 [18]. The antisite disorder in double perovskites has also been suggested to play an important role [16,20]. Laguna-Marco *et al.* suggest that the Ir^{4+} and Ir^{6+} magnetic impurities may locate in the antisite disorder region [20]. Condensation of $J = 1$ triplon excitations of $5d^4$ oxides is also a possible source for the observed magnetic moments [27,28]. Chen *et al.* proposed that the condensation is unlikely in Sr_2YIrO_6 and Ba_2YIrO_6 with the ideal crystal structure, but the antisite disorder between Y^{3+} and Ir^{5+} can break down the local nonmagnetic singlets [16]. Recent studies on A_2BIrO_6 (A = Ba, Sr; B = Lu, Sc) also support the $J = 0$ ground state for these Ir^{5+} oxides and indicate that the magnetic signals are from extrinsic sources, such as magnetic impurities and antisite disorder [21].

*Corresponding author: ygshi@iphy.ac.cn
†Corresponding author: hai.feng@iphy.ac.cn

To narrow down the possible explanations, it is better to consider studies on Ir^{5+} oxides with less antisite disorder. Recently, studies on K_4CdCl_6-type polycrystalline Ir^{5+} oxide Sr_3NaIrO_6 have been reported and indicate a possible quantum spin liquid ground state (reported $\mu_{\rm eff} = 0.49\,\mu_{\rm B}/{\rm Ir}$) [22]. In comparison with A_2YIrO_6 (A = Sr, Ba), where the $Ir^{5+}O_6$ octahedra are separated by $Y^{3+}O_6$, the $Ir^{5+}O_6$ octahedra are separated with $Na^{1+}O_6$ octahedra in the Sr_3NaIrO_6. The larger charge difference would reduce the antisite disorder between Na^{1+} and Ir^{5+} in Sr_3NaIrO_6 as compared with Sr_2YIrO_6 and Ba_2YIrO_6. Thus, the K_4CdCl_6-type iridate is a good platform to investigate the ground state of Ir^{5+} ions. To track the $J = 0$ ground state for Sr_3NaIrO_6, it is better to grow single crystals to minimize any by-phases and lattice defects. In this work, we successfully grow single crystals of K_4CdCl_6-type iridate oxides Sr_3NaIrO_6 and Sr_3AgIrO_6. Magnetic measurements reveal that the $\mu_{\rm eff}$ for Sr_3NaIrO_6 single crystals is about $0.31\mu_{\rm B}$ for $H\perp c$ and $0.28\mu_{\rm B}$ for $H||c$ which are smaller than that of $0.49\,\mu_{\rm B}$ reported for the polycrystalline Sr_3NaIrO_6 [22]. The presence of a few percent of magnetic Ir^{4+} impurity is indicated by the analysis of low-temperature specific heat data which is likely to fully explain the observed $\mu_{\rm eff}$, supporting the $J = 0$ ground state of Ir^{5+} in Sr_3NaIrO_6.

II. EXPERIMENT

The $SrOH \cdot 8H_2O$, NaOH, and Ir with a molar ratio of 3:50:1 (for Sr_3NaIrO_6) and $SrOH \cdot 8H_2O$, Ag_2O, and Ir with a molar ratio of 3:0.5:1 (for Sr_3AgIrO_6) were weighted, respectively. The mixtures were placed into Al_2O_3 crucibles with lids, then heated to 873 K for 1 h and annealed for 12 h before cooled to room temperature by stopping the heating. Single crystals were separated by washing with deionized water.

Single-crystal x-ray diffraction (SCXRD) measurements were conducted on a Bruker D8 Venture diffractometer at 300 K using Mo $K\alpha$ radiation ($\lambda = 0.71073$ Å). The frames were integrated with the Bruker SAINT software package using a narrow-frame algorithm. Data were corrected for absorption effects using the multiscan method (SADABS). The crystalline structures were refined by the full-matrix least-squares method on F^2 using the SHELXL-2018/3 program.

Single crystals of selected samples were used for magnetic susceptibility (χ), longitudinal resistivity ρ, specific heat, and x-ray absorption spectroscopy (XAS). The magnetic properties were measured under different applied magnetic fields in field-cooling (FC) and zero-field-cooling (ZFC) modes using a superconducting quantum interference device and vibrating-sample magnetometer in a magnetic properties measurement system (MPMS). Isothermal magnetization (M-H) was measured at several fixed temperatures. These transport measurements (both resistivity and specific heat) were measured by a physical property measurement system (Quantum Design) using the standard DC four-probe technique and a thermal relaxation method, respectively. XAS spectra at the Ir-L_3 edges were studied at the Taiwan Light Source (TLS) beamline 17C of the National Synchrotron Radiation Research Center (NSRRC).

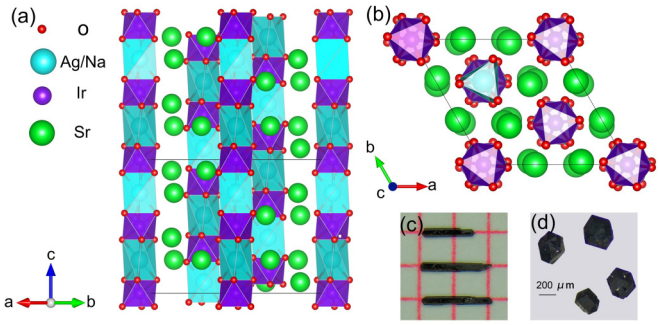

FIG. 1. Crystal structures of Sr_3AgIrO_6(Sr_3NaIrO_6) view along (a) [110] and (b) [001] directions. Panels (c) and (d) show optical photos of Sr_3NaIrO_6 and Sr_3AgIrO_6 single crystals, respectively.

III. RESULTS AND DISCUSSION

Single crystals for Sr_3NaIrO_6 with dimensions of ~2 mm × 0.3 mm × 0.3 mm and single crystals for Sr_3AgIrO_6 with ~0.3 mm × 0.3 mm × 0.3 mm were obtained as shown in Figs. 1(c) and 1(d), respectively. Analysis of the room temperature SCXRD data confirms that Sr_3NaIrO_6 and Sr_3AgIrO_6 crystallize in the K_4CdCl_6-type structure with the space group R-3c (no.167). The refined lattice parameters were $a = 9.6408(3)$Å and $c = 11.5508(5)$Å for Sr_3NaIrO_6 and $a = 9.5996(3)$Å and $c = 11.9032(6)$Å for Sr_3AgIrO_6. Detailed crystallographic data obtained from the SCXRD were summarized in Table I. The crystallographic information files for Sr_3NaIrO_6 and Sr_3AgIrO_6 are attached in the Supplemental Material [29].

In the crystal structures of Sr_3NaIrO_6 and Sr_3AgIrO_6, Na/Ag atoms occupy the 6a site, Ir atoms occupy the 6b site, Sr atoms occupy the 18e site, and O atoms occupy the 36f site (see Tables II and III). The crystal structure of Sr_3NaIrO_6 and Sr_3AgIrO is shown in Fig. 1. The IrO_6 octahedra are connected with NaO_6/AgO_6 octahedra through face sharing, forming one-dimensional chains. During the analysis of single crystal x-ray diffraction data, we checked the possibility of antisite between Na/Ag and Ir sites and found no indication of antisite disorder. The bond lengths for Ir-O are 1.984 and 1.989 Å for Sr_3NaIrO_6 and Sr_3AgIrO_6, respectively. The bond valence sum for Ir ions calculated from the Ir-O bond length is 4.99 and 4.92 for Sr_3NaIrO_6 and Sr_3AgIrO_6, respectively, which are close to the nominal Ir^{5+} oxidation states.

It is well known that hard x-ray absorption spectroscopy (XAS) at the 5d elements L edge is highly sensitive to their oxidation states, since the energy position of the strong white line shifts to higher energy by one or more eV with an increase of the valence state of 5d metal ion by 1 [30–34]. Figure 2 shows the Ir-L_3 XAS spectra for Sr_3NaIrO_6 and Sr_3AgIrO_6 together with the Ir^{4+} reference La_2CoIrO_6 and the Ir^{5+} reference Sr_2CoIrO_6 [35]. The energy position of Sr_3NaIrO_6 shifts about ~1.3 eV toward higher energy in comparison with La_2CoIrO_6, but locates at the same energy as that of Sr_2CoIrO_6, supporting the Ir^{5+} oxidation state. The energy position of Sr_3AgIrO_6 is a little lower than those of Sr_3NaIrO_6 and Sr_2CoIrO_6, and is about ~1 eV higher than La_2CoIrO_6, indicating that the oxidation state of the Ir ion in Sr_3AgIrO_6 is a little lower than +5. From these XAS spectra we can

TABLE I. Crystallographic and structure refinement data for Sr_3AgIrO_6 and Sr_3NaIrO_6.

Chemical formula	Sr_3AgIrO_6	Sr_3NaIrO_6
Formula weight	658.94 g/mol	574.05 g/mol
Radiation	Mo $K\alpha$, 0.710 73 Å	Mo $K\alpha$, 0.710 73 Å
Temperature	300 K	300 K
Crystal system	trigonal	trigonal
Space group	R-3c	R-3c
Unit cell dimensions	$a = 9.5996(3)$ Å	$a = 9.6408(3)$ Å
	$c = 11.9032(6)$ Å	$c = 11.5508(5)$ Å
Volume	949.95(8) Å^3	929.76(7) Å^3
Z	6	6
Density (calculated)	6.911 g/cm^3	6.152 g/cm^3
Absorption coefficient	49.048 mm^{-1}	47.117 mm^{-1}
No. reflections	5112	6376
No. independent reflections	265	261
No. observed reflections	256	256
F (000)	1716	1500
Theta range for data collection	4.21–28.29°	4.23–28.36°
Index ranges	$-12 \leqslant h \leqslant 12$	$-12 \leqslant h \leqslant 12$
	$-12 \leqslant k \leqslant 12$	$-12 \leqslant k \leqslant 11$
	$-15 \leqslant l \leqslant 15$	$-15 \leqslant l \leqslant 15$
Goodness of fit	1.265	1.118
$R1$ ($I > 2\sigma_1$)	0.0230	0.0103
$\omega R2$ ($I > 2\sigma_1$)	0.0735	0.0258
$R1$ (all data)	0.0237	0.0106
$\omega R2$ (all data)	0.0740	0.0261
Weighting scheme	$w = 1/[\sigma^2 F_o^2 + (0.0423P)^2 + 38.8002P]$	$w = 1/[\sigma^2 F_o^2 + (0.0141\,P)^2 + 6.8962\,P]$
	where $P = (F_o^2 + 2F_c^2)/3$	where $P = (F_o^2 + 2F_c^2)/3$
Refinement software	SHELXL-2018/3	SHELXL-2018/3

conclude that the oxidation state of Ir ion in Sr_3NaIrO_6 is Ir^{5+}, but we cannot exclude the presence of a few percent of Ir^{4+} or Ir^{6+} ions [35]. For Sr_3AgIrO_6, the average Ir oxidation state is a little lower than Ir^{5+} and a moderate amount of Ir^{4+} ions coexist with the major Ir^{5+} ions.

The temperature-dependent resistivity, $\rho(T)$, for Sr_3NaIrO_6 and Sr_3AgIrO_6 are shown in Figs. 3(a) and 3(b). The $\rho(T)$ curves show semiconducting behavior. The ρ increases with cooling and is out of range below 250 and 260 K for Sr_3NaIrO_6 and Sr_3AgIrO_6, respectively. The high-temperature data (>320 K) are used to estimate the gap according to the Arrhenius equation, $\rho \propto \exp^{E_a/2k_BT}$ [see the insets in Figs. 3(a) and 3(b)]. The estimated activation gap, E_a, is ~0.80 eV for Sr_3NaIrO_6 and ~0.58 eV for Sr_3AgIrO_6.

Single crystals of Sr_3NaIrO_6 are large enough (~2 mm along the c axis) to measure their anisotropic magnetic properties. The temperature-dependent magnetic susceptibility curves, $\chi(T)$, of Sr_3NaIrO_6 single crystals measured with magnetic fields perpendicular to the c axis ($H \perp c$) and parallel to the c axis ($H||c$) are shown in Figs. 4(a) and 4(b). The ZFC and FC curves are overlapping, and only FC curves are shown. There is no sign of magnetic order down to 2 K. The $\chi(T)$ data above 50 K can be fitted with the Curie-Weiss law, $\chi = \chi_0 + C/(T-\theta_W)$, where C, θ_W, and χ_0 are the Curie constant, Weiss temperature, and the temperature-independent component, respectively. For the case of $H \perp c$, the fitting results in a C of 0.012 emu mol^{-1} Oe^{-1} and a θ_W of −34 K. For the case of $H||c$, a C of 0.008 emu mol^{-1} Oe^{-1} and a θ_W of 1 K is obtained from the fitting. The χ_0 values for Sr_3NaIrO_6 are 6.2×10^{-4} and 5.4×10^{-4} emu mol^{-1} Oe^{-1} for $H \perp c$ and $H||c$, respectively. The μ_{eff} calculated from the C is about $0.31\mu_B$ for $H \perp c$ and $0.28\mu_B$ for $H||c$.

Regarding the Sr_3AgIrO_6 single crystals, anisotropic magnetic measurement is not possible due to their small size (~300 μm) and crystal morphology. A total weight of ~19-mg Sr_3AgIrO_6 single crystals were collected without orientation for magnetic measurement. The $\chi(T)$ curves measured under varied H for Sr_3AgIrO_6 single crystals without

TABLE II. Refined atomic positions and temperature parameters for Sr_3NaIrO_6.

Atom	x	y	z	Occupancy	U_{eq}(Å^2)	Site
Ir1	2/3	1/3	5/6	1	0.00379(9)	6b
O1	0.4882(2)	0.3102(2)	0.7336(2)	1	0.0075(4)	36f
Sr1	0.3090(1)	1/3	7/12	1	0.0069(1)	18e
Na1	2/3	1/3	7/12	1	0.0090(6)	6a

TABLE III. Refined atomic positions and temperature parameters for Sr_3AgIrO_6.

Atom	x	y	z	Occupancy	U_{eq}(Å^2)	Site
Ir1	2/3	1/3	1/3	1	0.0061(3)	6*b*
O1	0.6896(7)	0.5138(6)	0.2373(4)	1	0.0099(10)	36*f*
Sr1	0.6896(1)	2/3	5/12	1	0.0094(3)	18*e*
Ag1	2/3	1/3	1/12	1	0.0230(5)	6*a*

orientation are shown in Fig. 4(c). Only FC curves are shown because the ZFC and FC curves are overlapping. There is no sign of magnetic order down to 2 K. The $\chi(T)$ data above 50 K can also be fitted with the Curie-Weiss law, resulting in a χ_0 of 3.27×10^{-4} emu mol^{-1} Oe^{-1}, C of 0.04 emu mol^{-1} Oe^{-1}, and a θ_W of -35 K. The μ_{eff} calculated from the C is 0.57 μ_B.

Figure 5 shows the $C_p(T)$ curves of Sr_3NaIrO_6 and Sr_3AgIrO_6. There is no indication of magnetic order down to 1.8 K for Sr_3NaIrO_6 and Sr_3AgIrO_6. The low-temperature C_p/T vs T^2 data, shown in the insets in Fig. 5, show rough linear behaviors except for the upturns at the lowest temperatures. The linear parts were analyzed with the approximated Debye model, $C_p/T = \gamma + \beta T^2$, where the γ is the electronic specific heat coefficient and the β is related to the Debye temperature. Fitting of the linear parts results in a $\gamma = 0.07$ mJ mol^{-1} K^{-2} and $\beta = 2.64 \times 10^{-4}$ J mol^{-1} K^{-4} for Sr_3NaIrO_6 and $\gamma = 3.0$ mJ mol^{-1} K^{-2} and $\beta = 9.05 \times 10^{-4}$ J mol^{-1} K^{-4} for Sr_3AgIrO_6. The small γ value indicates the vanishing of the density of states, which is consistent with the insulating nature of Sr_3NaIrO_6 and Sr_3AgIrO_6.

The low-temperature C_p/T vs T curves measured without and with varied magnetic fields are shown in Figs. 6(a) and 6(b) for Sr_3NaIrO_6 and Sr_3AgIrO_6, respectively. The C_p/T vs T curves measured without fields show small anomalies below ~3.5 K. These anomalies shift towards higher temperatures and broaden with increasing applied magnetic fields, suggesting their magnetic origin. To estimate the magnetic contribution (C_{mag}), we subtract the $C_p(T)$ data below 12 K measured under 90 kOe with an estimated lattice contribution $C_{lat} = \gamma T + \beta T^3$, and the resulting C_{mag}/T vs T curves are shown in Figs. 6(c) and 6(d) for Sr_3NaIrO_6 and Sr_3AgIrO_6, respectively. These curves show broad maximums around 3–4 K for Sr_3NaIrO_6 and Sr_3AgIrO_6. It should be noted that these values may be underestimated because the entropy below 1.8 K is not counted in these cases. The estimated magnetic entropy (S_{mag}) for Sr_3NaIrO_6 and Sr_3AgIrO_6 is about 0.06 and 0.33 J mol^{-1} K^{-1}, respectively. Assuming these magnetic contributions are from Ir^{4+} impurities, these values are about ~1.7% and ~9.2%, respectively, of the averaged entropy $S_{mag} = 3.6$ J mol^{-1} K^{-1} reported for the Ir^{4+} double perovskite La_2MgIrO_6 and La_2ZnIrO_6 [36]. These results are consistent with the XAS results that the Ir ions in Sr_3NaIrO_6 are Ir^{5+} (but cannot exclude the presence of a few percent of magnetic Ir^{4+} or/and Ir^{6+}) while a moderate amount of Ir^{4+} ions coexists with the Ir^{5+} ions in Sr_3AgIrO_6.

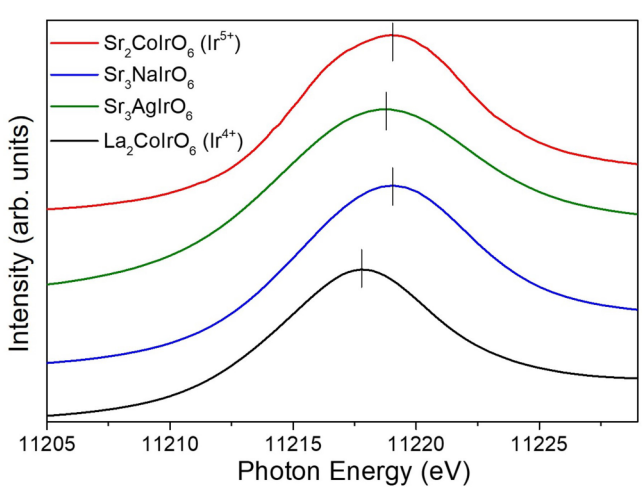

FIG. 2. Ir-L_3 XAS spectra of Sr_3NaIrO_6 and Sr_3AgIrO_6 in comparison with an Ir^{4+} reference La_2CoIrO_6 and an Ir^{5+} reference Sr_2CoIrO_6.

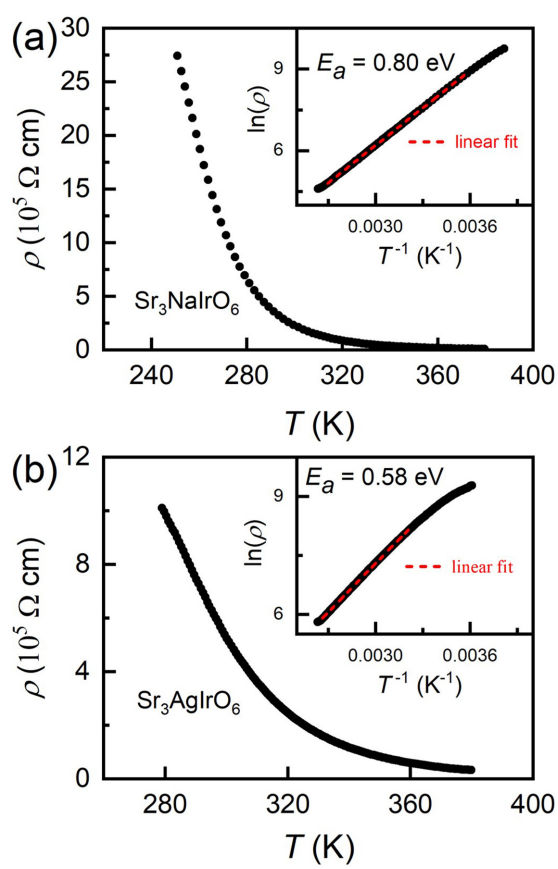

FIG. 3. The temperature dependence of resistivity for (a) Sr_3NaIrO_6 and (b) Sr_3AgIrO_6. The insets show corresponding data fitted with the Arrhenius equation.

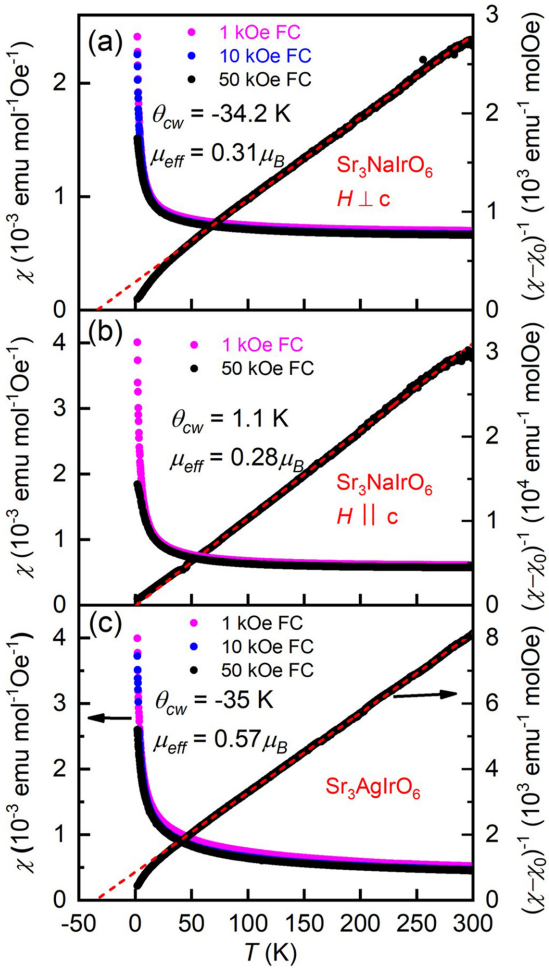

FIG. 4. Temperature dependence of magnetic susceptibility and the inverse magnetic susceptibility for (a) Sr_3NaIrO_6 ($H \perp c$), (b) Sr_3NaIrO_6 ($H||c$), and (c) Sr_3AgIrO_6.

The $\mu_{\rm eff}$, $\theta_{\rm W}$, and χ_0 values for Sr_3NaIrO_6 and Sr_3AgIrO_6 reported in this work are summarized in Table IV in comparison with other Ir^{5+} oxides crystalizing in double perovskite or K_4CdCl_6-type structures. The χ_0 summarized in Table IV are of the magnitude of 10^{-4} emu mol^{-1} Oe^{-1}. The χ_0 reported in this work for Sr_3NaIrO_6 and Sr_3AgIrO_6 single crystals are in the reported range. Except for the large $\mu_{\rm eff}$ of 0.91 $\mu_{\rm B}$/Ir and of 1.44 $\mu_{\rm B}$/Ir once reported for Sr_2YIrO_6 [11] and Ba_2YIrO_6 [12], respectively, other studies on Sr_2YIrO_6, Ba_2YIrO_6, and the other Ir^{5+} double perovskite and K_4CdCl_6-type oxides reveal relatively small $\mu_{\rm eff}$ values of 0.19–0.63 $\mu_{\rm B}$/Ir [13–25]. The $\mu_{\rm eff}$ values for single crystals of Sr_3NaIrO_6 and Sr_3AgIrO_6 in this work are within this range.

In comparison with polycrystalline Sr_3NaIrO_6 (0.49 $\mu_{\rm B}$/Ir), the observed $\mu_{\rm eff}$ values for Sr_3NaIrO_6 single crystal (0.31$\mu_{\rm B}$/Ir for $H \perp c$ and 0.28$\mu_{\rm B}$/Ir for $H||c$) are reduced. The valence state is also confirmed to be mainly Ir^{5+} in polycrystalline Sr_3NaIrO_6 [22]. Thus, the reduction of $\mu_{\rm eff}$ for the single crystal samples may be related to the decrease of by-phases and lattice defects because in polycrystalline samples synthesized by solid-state reactions it is difficult to avoid the minute number of by-phases and they usually have more lattice defects than the single crystal samples.

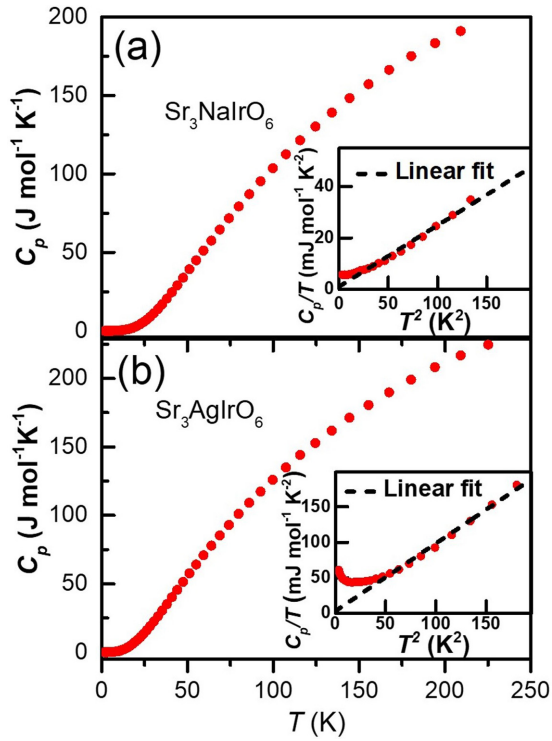

FIG. 5. Temperature dependence of specific heat C_p for (a) Sr_3NaIrO_6 and (b) Sr_3AgIrO_6. The insets show the corresponding C_p/T vs T^2 curves.

Though our XAS spectra confirm that the oxidation state of Ir in Sr_3NaIrO_6 is mainly Ir^{5+}, one cannot exclude the presence of a few percent of magnetic Ir^{4+} or/and Ir^{6+} ions. The presence of Ir^{4+} and/or Ir^{6+} magnetic defects has been confirmed in Sr_2YIrO_6 [20], Sr_2CoIrO_6 [35], and Ba_2YIrO_6 [18]. Studies on Ir^{4+} double perovskites La_2ZnIrO_6 and La_2MgIrO_6 have reported $\mu_{\rm eff}$ values of 1.71 $\mu_{\rm B}$ and 1.42 $\mu_{\rm B}$, respectively, which are close to the theoretical value of 1.73 $\mu_{\rm B}$ for Ir^{4+} ($J = 1/2$) [36]. If we assume

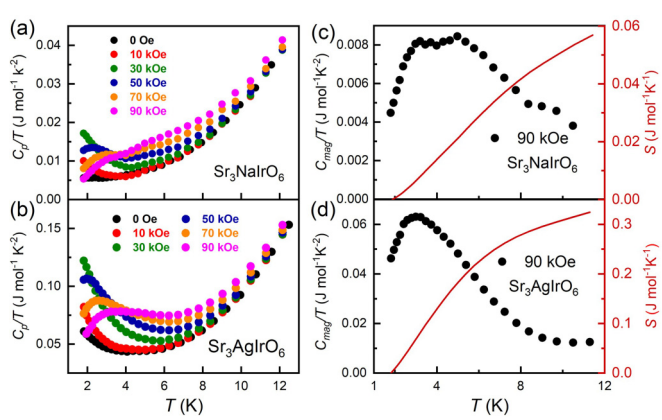

FIG. 6. Temperature-dependent C_p/T data under varied magnetic fields for (a) Sr_3NaIrO_6 and (b) Sr_3AgIrO_6. Temperature-dependent $C_{\rm mag}/T$ and $S_{\rm mag}$ data for (c) Sr_3NaIrO_6 and (d) Sr_3AgIrO_6.

TABLE IV. Magnetic properties of Ir^{5+} oxides with double perovskite (DP) and K_4CdCl_6 structures.

Material	Crystal structure	χ_0 (10^{-4} emu mol^{-1} Oe^{-1})	μ_{eff} (μ_B/Ir)	θ_W (K)	Reference
Ba_2YIrO_6	DP		0.3	−10	[15]
Ba_2YIrO_6	DP	4.8	0.63	−5	[16]
Ba_2YIrO_6	DP	5.4	0.52	−4	[16]
Ba_2YIrO_6	DP	5.4	0.50	−8	[16]
Ba_2YIrO_6	DP	5.83	0.44	−8.9	[13]
Ba_2YIrO_6	DP		0.31		[17]
Ba_2YIrO_6	DP		0.48	−16	[18]
Ba_2YIrO_6	DP	−3.9	1.44	−149	[12]
$Ba_{1.26}Sr_{0.74}YIrO_6$	DP	4.4	0.64	−18	[12]
$Ba_{2-x}Sr_xYIrO_6$	DP		0.47		[19]
Sr_2YIrO_6	DP		0.91	−229	[11]
Sr_2YIrO_6	DP	5.90	0.21	−2.8	[14]
Sr_2YIrO_6	DP		0.3		[20]
$Sr_{1.6}Ca_{0.4}YIrO_6$	DP		0.6		[20]
Sr_2LuIrO_6	DP	5.49	0.27	−2.55	[21]
Ba_2LuIrO_6	DP	4.98	0.42	−13.2	[21]
Sr_2ScIrO_6	DP	5.43	0.32	−10.7	[21]
Ba_2ScIrO_6	DP	5.10	0.48	−18.7	[21]
Bi_2NaIrO_6	DP	6.3	0.19	−6.8	[23]
$LaSrMgIrO_6$	DP	3.5	0.61	7	[24]
$LaSrZnIrO_6$	DP	3.9	0.46	1	[24]
Sr_3NaIrO_6	K_4CdCl_6		0.49	−23.6	[22]
Sr_3LiIrO_6	K_4CdCl_6		0.4	−21	[25]
Sr_3LiIrO_6	K_4CdCl_6		0.45	−71	[25]
Sr_3NaIrO_6	K_4CdCl_6	6.2	0.31($H\perp c$)	−34	this work
		5.4	0.28($H\|\|c$)	1	
Sr_3AgIrO_6	K_4CdCl_6	3.3	0.57	−35	this work

the observed $\mu_{eff} \approx 0.3\mu_B$ for Sr_3NaIrO_6 single crystals is solely contributed from magnetic Ir^{4+} ($\mu_{eff} = 1.73\,\mu_B$) while Ir^{5+} ions are nonmagnetic ($J = 0$), there should be about ∼3.0% of Ir^{4+} magnetic impurities according to $\mu_{eff}^2 = (1-x)(\mu_{eff}\text{-}Ir^{5+})^2 + x(\mu_{eff}\text{-}Ir^{4+})^2$. The existence of magnetic Ir^{4+} with a low limit of ∼1.7% for Sr_3NaIrO_6 is suggested from the analysis of low-temperature $C_p(T)$ data, which is not far from the theoretical amount of ∼3.0%.

In comparison with Sr_3NaIrO_6, the average valence state of Ir in Sr_3AgIrO_6 is a little lower than Ir^{5+}, indicating the presence of a moderate amount of Ir^{4+} ions. The presence of magnetic Ir^{4+} with a low limit of ∼9.2% is estimated for Sr_3AgIrO_6 by the analysis of the low-temperature $C_p(T)$ data. The observed μ_{eff} for Sr_3AgIrO_6 single crystals is ∼0.57 μ_B. Assuming the observed μ_{eff} of 0.57 μ_B for Sr_3AgIrO_6 is solely contributed from magnetic Ir^{4+} while Ir^{5+} ions are nonmagnetic, there should be about ∼10.9% of magnetic Ir^{4+} according to $\mu_{eff}^2 = (1x)(\mu_{eff}\text{-}Ir^{5+})^2 + x(\mu_{eff}\text{-}Ir^{4+})^2$, which is comparable to the low limit of Ir^{4+} (∼9.2%) estimated from $C_p(T)$ data of Sr_3AgIrO_6 single crystals.

In comparison with A_2YIrO_6 (A = Sr, Ba), where the $Ir^{5+}O_6$ octahedra are separated by $Y^{3+}O_6$, and the $Ir^{5+}O_6$ octahedra are separated by $Na^{1+}O_6/Ag^{1+}O_6$ octahedra along the one-dimensional chain in Sr_3NaIrO_6 and Sr_3AgIrO_6. The much larger charge difference would significantly reduce the antisite disorder between Na^{1+}/Ag^{1+} and Ir^{5+} in Sr_3NaIrO_6 and Sr_3AgIrO_6 as compared with Sr_2YIrO_6 and Ba_2YIrO_6. Thus, the contributions to the magnetic moment from antisite disorder as discussed for Sr_2YIrO_6 and Ba_2YIrO_6 should be much reduced in Sr_3NaIrO_6 and Sr_3AgIrO_6.

From these analyses, the paramagnetic moments observed in Sr_3NaIrO_6 and Sr_3NaIrO_6 single crystals are likely contributed solely by the magnetic Ir^{4+}, supporting the $J = 0$ ground state for Ir^{5+}. This is consistent with the studies on Ir^{5+} double perovskites A_2BIrO_6 (A = Ba, Sr; B = Y, Lu, Sc) which support the $J = 0$ ground state for Ir^{5+} and indicate the magnetic moments are from extrinsic sources [14,17,18,20,21]. Studies on the layered oxide $Sr_2Co_{0.5}Ir_{0.5}O_4$ also support the $J = 0$ ground state for Ir^{5+} and show that the energy gap between the singlet state and the excited triplet state is large [37]. The presence of magnetic Ir^{4+} indicates that a small number of oxygen vacancies exist in our Sr_3NaIrO_6 and Sr_3AgIrO_6 single crystals. The possibility of thermodynamic instability of stoichiometric Ir^{5+} oxides and a partial reduction of Ir^{5+} to Ir^{4+} has been suggested by Jansen *et al.* [23].

It should be noted that the θ_W values are anisotropic in our magnetic measurements on Sr_3NaIrO_6 single crystals. For the polycrystalline Sr_3NaIrO_6, the reported θ_W is −23.6 K. For our Sr_3NaIrO_6 single crystals, the θ_W is about 1 K for the case of $H||c$ but is about −34 K for $H\perp c$, indicating that the magnetic exchange interactions are negligible along the one-dimensional chain ($H||c$) and are mainly for interchains ($H\perp c$). In the ideal Sr_3NaIrO_6 structure, there is no direct

superexchange Ir-O-Ir path, and the magnetic exchange interactions are mediated by the extended superexchange path Ir-O-O-Ir [38,39]. The nearest Ir-Ir is about 5.78 Å along the chain which is a little bit shorter than the length of 5.89 Å for interchains, but the nearest O-O distance between nearest IrO_6 octahedra along the one-dimensional chain (3.50 Å) is much longer than that of 2.99 Å for interchains, which may be responsible for the magnetic exchange interactions being mainly for interchains in the Sr_3NaIrO_6 single crystals.

IV. CONCLUSIONS

Single crystals of Sr_3NaIrO_6 and Sr_3AgIrO_6 have been successfully grown using hydroxides flux. Analysis of room temperature SCXRD data found that Sr_3NaIrO_6 and Sr_3AgIrO_6 crystallize in the K_4CdCl_6-type structure with the space group R-3c (no. 167). Sr_3NaIrO_6 and Sr_3AgIrO_6 are electrically insulating with estimated activation gaps of 0.68 and 0.80 eV, respectively. The magnetic results show paramagnetism down to 2 K for both Sr_3NaIrO_6 and Sr_3AgIrO_6. In comparison with polycrystalline Sr_3NaIrO_6 (0.49 μ_B), our Sr_3NaIrO_6 single crystals display smaller μ_{eff} values (0.31μ_B for $H \perp c$ and 0.28μ_B for $H||c$). The μ_{eff} for Sr_3AgIrO_6 single crystals is about 0.57 μ_B. Combined analyses of the XAS spectra and the low-temperature $C_p(T)$ data indicate that the Ir ions are mainly Ir^{5+} in Sr_3NaIrO_6 but there is a low limit of ~1.7% of magnetic Ir^{4+} ions. For Sr_3AgIrO_6, the Ir ions are a little lower than Ir^{5+} and it contains magnetic impurity Ir^{4+} with a low limit of ~9.2%. The magnetic impurities are likely to fully explain the observed μ_{eff} values for Sr_3NaIrO_6 and Sr_3AgIrO_6 single crystals, supporting the $J = 0$ ground state for Ir^{5+} in Sr_3NaIrO_6 and Sr_3AgIrO_6.

ACKNOWLEDGMENTS

H.L.F. thanks Professor L. H. Tjeng for insightful comments. This work was supported by the Beijing Natural Science Foundation (Grant No. Z180008), the National Natural Science Foundation of China (Grants No. 12104492 and No. U2032204), the National Key Research and Development Program of China (Grants No. 2021YFA1400401 and No. 2017YFA0302900), the Strategic Priority Research Program of the Chinese Academy of Sciences (Grant No. XDB33010000), the K. C. Wong Education Foundation (Grant No. GJTD-2018-01), and the Informatization Plan of Chinese Academy of Sciences (Grant No. CAS-WX2021SF-0102). We also acknowledge support from the Max Planck-POSTECH-Hsinchu Center for Complex Phase Materials.

[1] I. H. Inoue, I. Hase, Y. Aiura, A. Fujimori, Y. Haruyama, T. Maruyama, and Y. Nishihara, Systematic Development of the Spectral Function in the $3d^1$ Mott-Hubbard System $Ca_{1-x}Sr_xVO_3$, Phys. Rev. Lett. **74**, 2539 (1995).

[2] A. E. Bocquet, T. Mizokawa, T. Saitoh, H. Namatame, and A. Fujimori, Electronic structure of 3d-Transition-Metal compounds by analysis of the 2p core-level photoemission spectra, Phys. Rev. B **46**, 3771 (1992).

[3] I. S. Lyubutin, S. G. Ovchinnikov, A. G. Gavriliuk, and V. V. Struzhkin, Spin-Crossover-Induced mott transition and the other scenarios of metallization in $3d^n$ metal compounds, Phys. Rev. B **79**, 085125 (2009).

[4] L. Huang, T. Ayral, S. Biermann, and P. Werner, Extended dynamical mean-field study of the hubbard model with long-range interactions, Phys. Rev. B **90**, 195114 (2014).

[5] F. Aryasetiawan, K. Karlsson, O. Jepsen, and U. Schönberger, Calculations of hubbard u from first-principles, Phys. Rev. B **74**, 125106 (2006).

[6] W. Witczak-Krempa, G. Chen, Y. B. Kim, and L. Balents, Correlated quantum phenomena in the strong spin-orbit regime, Annu. Rev. Condens. Matter Phys. **5**, 57 (2014).

[7] J. G. Rau, E. K.-H. Lee, and H.-Y. Kee, Spin-Orbit physics giving rise to novel phases in correlated Systems: iridates and related materials, Annu. Rev. Condens. Matter Phys. **7**, 195 (2016).

[8] S. J. Moon, H. Jin, K. W. Kim, W. S. Choi, Y. S. Lee, J. Yu, G. Cao, A. Sumi, H. Funakubo, C. Bernhard, and T. W. Noh, Dimensionality-Controlled Insulator-Metal Transition and Correlated Metallic State in 5 D Transition Metal Oxides $Sr_{n+1}Ir_nO_{3n+1}$ (n = 1, 2, and ∞), Phys. Rev. Lett. **101**, 226402 (2008).

[9] B. J. Kim, H. Jin, S. J. Moon, J.-Y. Kim, B.-G. Park, C. S. Leem, J. Yu, T. W. Noh, C. Kim, S.-J. Oh, J.-H. Park, V. Durairaj, G. Cao, and E. Rotenberg, Novel $J_{eff} = 1/2$ Mott State Induced by Relativistic Spin-Orbit Coupling in Sr_2IrO_4, Phys. Rev. Lett. **101**, 076402 (2008).

[10] A. E. Taylor, S. Calder, R. Morrow, H. L. Feng, M. H. Upton, M. D. Lumsden, K. Yamaura, P. M. Woodward, and A. D. Christianson, Spin-Orbit Coupling Controlled $J = 3/2$ Electronic Ground State in $5d^3$ Oxides, Phys. Rev. Lett. **118**, 207202 (2017).

[11] G. Cao, T. F. Qi, L. Li, J. Terzic, S. J. Yuan, L. E. DeLong, G. Murthy, and R. K. Kaul, Novel Magnetism of Ir^{5+} ($5d^4$) Ions in the Double Perovskite Sr_2YIrO_6, Phys. Rev. Lett. **112**, 056402 (2014).

[12] J. Terzic, H. Zheng, F. Ye, H. D. Zhao, P. Schlottmann, L. E. De Long, S. J. Yuan, and G. Cao, Evidence for a low-temperature magnetic ground state in double-perovskite iridates with Ir^{5+} ($5d^4$) ions, Phys. Rev. B **96**, 064436 (2017).

[13] T. Dey, A. Maljuk, D. V. Efremov, O. Kataeva, S. Gass, C. G. F. Blum, F. Steckel, D. Gruner, T. Ritschel, A. U. B. Wolter, J. Geck, C. Hess, K. Koepernik, J. van den Brink, S. Wurmehl, and B. Büchner, Ba_2YIrO_6: a cubic double perovskite material with Ir^{5+} ions, Phys. Rev. B **93**, 014434 (2016).

[14] L. T. Corredor, G. Aslan-Cansever, M. Sturza, K. Manna, A. Maljuk, S. Gass, T. Dey, A. U. B. Wolter, O. Kataeva, A. Zimmermann, M. Geyer, C. G. F. Blum, S. Wurmehl, and B. Buchner, Iridium double perovskite Sr_2YIrO_6: a combined structural and specific heat study, Phys. Rev. B **95**, 064418 (2017).

[15] A. Nag, S. Bhowal, A. Chakraborty, M. M. Sala, A. Efimenko, F. Bert, P. K. Biswas, A. D. Hillier, M. Itoh, S. D. Kaushik,

V. Siruguri, C. Meneghini, I. Dasgupta, and S. Ray, Origin of magnetic moments and presence of spin-orbit singlets in Ba_2YIrO_6, Phys. Rev. B **98**, 014431 (2018).

[16] Q. Chen, C. Svoboda, Q. Zheng, B. C. Sales, D. G. Mandrus, H. D. Zhou, J.-S. Zhou,D. McComb, M. Randeria, N. Trivedi, and J.-Q. Yan, Magnetism out of antisite disorder in the $j = 0$ compound Ba_2YIrO_6, Phys. Rev. B **96**, 144423 (2017).

[17] F. Hammerath, R. Sarkar, S. Kamusella, C. Baines, H.-H. Klauss, T. Dey, A. Maljuk, S. Gaß, A. U. B. Wolter, H.-J. Grafe, S. Wurmehl, and B. Büchner, Diluted paramagnetic impurities in nonmagnetic Ba_2YIrO_6, Phys. Rev. B **96**, 165108 (2017).

[18] S. Fuchs, T. Dey, G. Aslan-Cansever, A. Maljuk, S. Wurmehl, B. Büchner, and V. Kataev, Unraveling the Nature of Magnetism of the $5d^4$ Double Perovskite Ba_2YIrO_6, Phys. Rev. Lett. **120**, 237204 (2018).

[19] B. F. Phelan, E. M. Seibel, D. Badoe, W. Xie, and R. J. Cava, Influence of structural distortions on the ir magnetism in $Ba_{2-x}Sr_xYIrO_6$ double perovskites, Solid State Commun. **236**, 37 (2016).

[20] M. A. Laguna-Marco, E. Arias-Egido, C. Piquer, V. Cuartero, L. Hernández-López, P. Kayser, J. A. Alonso, J. A. T. Barker, G. Fabbris, C. A. Escanhoela Jr., and T. Irifune, Magnetism of Ir^{5+}-based double Perovskites: unraveling its nature and the influence of structure, Phys. Rev. B **101**, 014449 (2020).

[21] A. A. Aczel, Q. Chen, J. P. Clancy, C. dela Cruz, D. Reig-i-Plessis, G. J. MacDougall, C. J. Pollock, M. H. Upton, T. J. Williams, N. LaManna, J. P. Carlo, J. Beare, G. M. Luke, and H. D. Zhou, Spin-Orbit Coupling Controlled Ground States in the Double Perovskite Iridates A_2BIrO_6 (A = Ba, Sr; B = Lu, Sc), Phys. Rev. Mater. **6**, 094409 (2022).

[22] A. Bandyopadhyay, A. Chakraborty, S. Bhowal, V. Kumar, M. M. Sala, A. Efimenko, F. Bert, P. K. Biswas, C. Meneghini, N. Büttgen, I. Dasgupta, T. Saha Dasgupta, A. V. Mahajan, and S. Ray, Breakdown of atomic spin-orbit coupling picture in an apparently isolated pseudo-one-dimensional Iridate: Sr_3NaIrO_6, Phys. Rev. B **105**, 104431 (2022).

[23] B. E. Prasad, T. Doert, C. Felser, and M. Jansen, On $j_{\rm eff} = 0$ ground state Iridates(V): tracking residual paramagnetism in new Bi_2NaIrO_6, Chem. Eur. J. **24**, 16762 (2018).

[24] K. K. Wolff, S. Agrestini, A. Tanaka, M. Jansen, and L. H. Tjeng, Comparative study of potentially $j_{\rm eff} = 0$ ground state Iridium(V) in $SrLaNiIrO_6$, $SrLaMgIrO_6$, and $SrLaZnIrO_6$: comparative study of potentially $j_{\rm eff} = 0$ ground state Iridium(V) in $SrLaNiIrO_6$, $SrLaMgIrO_6$, and $SrLaZnIrO_6$, Z. Anorg. Allg. Chem. **643**, 2095 (2017).

[25] A. Bandyopadhyay, A. Chakraborty, S. Bhowal, V. Kumar, M. M. Sala, A. Efimenko, C. Meneghini, I. Dasgupta, T. Saha Dasgupta, A. V. Mahajan, and S. Ray, Sr_3LiIrO_6: A Potential Quantum Spin Liquid Candidate in the One Dimensional d^4 Iridate Family, arXiv:2111.00925.

[26] B. Ranjbar, E. Reynolds, P. Kayser, B. J. Kennedy, J. R. Hester, and J. A. Kimpton, Structural and magnetic properties of the iridium double perovskites $Ba_{2-x}Sr_xYIrO_6$, Inorg. Chem. **54**, 10468 (2015).

[27] G. Khaliullin, Excitonic Magnetism in Van Vleck–Type D^4 Mott Insulators, Phys. Rev. Lett. **111**, 197201 (2013).

[28] O. N. Meetei, W. S. Cole, M. Randeria, and N. Trivedi, Novel magnetic state in d^4 mott insulators, Phys. Rev. B **91**, 054412 (2015).

[29] See Supplemental Material at http://link.aps.org/supplemental/10.1103/PhysRevMaterials.6.094415 for the crystallographic information files (Cif) for Sr_3NaIrO_6 and Sr_3AgIrO_6.

[30] S. J. Mugavero, M. D. Smith, W.-S. Yoon, and H.-C. zur Loye, $Nd_2K_2IrO_7$ and $Sm_2K_2IrO_7$: Iridium(VI) oxides prepared under ambient pressure, Angew. Chem. Int. Ed. **48**, 215 (2009).

[31] J. Chen, X. Wang, Z. Hu, L. H. Tjeng, S. Agrestini, M. Valvidares, L. Nataf, K. Chen, F. Baudelet, M. Nagao, Y. Inaguma, A. A. Belik, Y. Tsujimoto, Y. Matsushita, T. Kolodiazhnyi, R. Sereika, M. Tanaka, and K. Yamaura, Enhanced magnetization of the Highest-T_C ferrimagnetic oxide Sr_2CrOsO_6, Phys. Rev. B **102**, 184418 (2020).

[32] Y.-Y. Chin, H.-J. Lin, Z. Hu, C.-Y. Kuo, D. Mikhailova, J.-M. Lee, S.-C. Haw, S.-A. Chen, H. Ishii, W. Schnelle, Y.-Fa. Liao, N. Hiraoka, K.-D. Tsuei, A. Tanaka, L. H. Tjeng, C.-T. Chen, and J.-M. Chen, Relation between the Co-O bond lengths and the spin state of co in layered Cobaltates: a high-pressure study, Sci Rep. **7**, 3656 (2017).

[33] H. L. Feng, S. Calder, M. P. Ghimire, Y.-H. Yuan, Y. Shirako, Y. Tsujimoto, Y. Matsushita, Z. Hu, C.-Y. Kuo, L. H. Tjeng, T.-W. Pi, Y.-L. Soo, J. F. He, M. Tanaka, Y. Katsuya, M. Richter, and K. Yamaura, Ba_2NiOsO_6: a dirac-mott insulator with ferromagnetism near 100 k, Phys. Rev. B **94**, 235158 (2016).

[34] K. Baroudi, C. Yim, H. Wu, Q. Huang, J. H. Roudebush, H.-J. Grafe, E. Vavilova, V. Kataev, B. Buechner, H. Ji, C. Kuo, Z. Hu, T.-W. Pi, C. Pao, J. Lee, D. Mikhailova, L. H. Tjeng, and R. J. Cava, Structure and properties of α-$NaFeO_2$-Type ternary sodium iridates, J. Solid State Chem. **210**, 195 (2014).

[35] S. Agrestini, K. Chen, C.-Y. Kuo, L. Zhao, H.-J. Lin, C.-T. Chen, A. Rogalev, P. Ohresser, T.-S. Chan, S.-C. Weng, G. Auffermann, A. Völzke, A. C. Komarek, K. Yamaura, M. W. Haverkort, Z. Hu, and L. H. Tjeng, Nature of the magnetism of iridium in the double perovskite Sr_2CoIrO_6, Phys. Rev. B **100**, 014443 (2019).

[36] G. Cao, A. Subedi, S. Calder, J.-Q. Yan, J. Yi, Z. Gai, L. Poudel, D. J. Singh, M. D. Lumsden, A. D. Christianson, B. C. Sales, and D. Mandrus, Magnetism and electronic structure of La_2ZnIrO_6 and La_2MgIrO_6: candidate $j_{\rm eff} = 1/2$ mott insulators, Phys. Rev. B **87**, 155136 (2013).

[37] S. Agrestini, C.-Y. Kuo, K. Chen, Y. Utsumi, D. Mikhailova, A. Rogalev, F. Wilhelm, T. Förster, A. Matsumoto, T. Takayama, H. Takagi, M. W. Haverkort, Z. Hu, and L. H. Tjeng, Probing the $j_{\rm eff} = 0$ ground state and the van vleck paramagnetism of the Ir^{5+} ions in layered $Sr_2Co_{0.5}Ir_{0.5}O_4$, Phys. Rev. B **97**, 214436 (2018).

[38] Y. Shi, Y. Guo, S. Yu, M. Arai, A. Sato, A. A. Belik, K. Yamaura, and E. Takayama-Muromachi, Crystal growth and structure and magnetic properties of the 5d oxide Ca_3LiOsO_6: extended superexchange magnetic interaction in oxide, J. Am. Chem. Soc. **132**, 8474 (2010).

[39] S. Calder, M. D. Lumsden, V. O. Garlea, J. W. Kim, Y. G. Shi, H. L. Feng, K. Yamaura, and A. D. Christianson, Magnetic structure determination of Ca_3LiOsO_6 using neutron and x-ray scattering, Phys. Rev. B **86**, 054403 (2012).